Numerical Simulations of Sand Production in Interbedded Hydrate-Bearing Sediments during Depressurization

Shun Uchida[1,4]*, Jeen-Shang Lin[2,4], Evgeniy M. Myshakin[3,4], Yongkoo Seol[4], Timothy S. Collett[5], Ray Boswell[4]
[1]Rensselaer Polytechnic Institute, United States; [2]University of Pittsburgh, United States; [3]AECOM,United States; [4]U.S. Department of Energy, National Energy Technology Laboratory, United States; [5]U.S. Geological Survey, United States
*Corresponding author: uchids@rpi.edu

Abstract

Geomechanical behavior of hydrate-bearing sediments during gas production is complex, involving changes in hydrate-dependent mechanical properties. When interbedded clay layers are present, the complexity is more pronounced because hydrate dissociation tends to occur preferentially in the sediments adjacent to the clay layers due to clay layers acting as a heat source. This would potentially lead to shearing deformation along the sand/clay contacts and may contribute to solid migration, which hindered past field-scale gas production tests. This paper presents a near-wellbore simulation of sand/clay interbedded hydrate-bearing sediments that have been subjected to depressurization and discusses the effect of clay layers on sand production.

Introduction

For a successful long-term gas production from gas hydrate-bearing sediments in the field, it is essential to better understand the responses of the sediments during gas extraction. Gas hydrate-bearing sediments undergo highly coupled multiphysics changes in thermal, hydrological and, most importantly from wellbore stability viewpoints, mechanical characteristics when subjected to depressurization. In previous field-scale gas hydrate production tests, the sediments exhibited uncontrolled sand production, resulting in premature termination of the well tests [1-2]. Motivated by these incidents, Uchida et al. [3] developed an analytical thermo-hydro-mechanical sand production model in gas hydrate-bearing sediments and showed the responses of simple homogenous hydrate-bearing sediments subjected to depressurization. Since hydrate-bearing sediments in real fields are not homogeneous, using the model, this paper investigates the responses of more representative hydrate-bearing sediments, that is, sand/clay interbedded hydrate-bearing sediments through near-wellbore numerical analyses. The conditions considered in this study correspond to a large-scale reservoir model presented in a companion paper [4]. A particular focus is placed on the effect of existing thin clay layer within thick clean sandy sediments on sand production.

Modeling procedure

Thermo-hydro-mechanical sand production model

This study adopts the thermo-hydro-mechanical sand production model developed by Uchida et al. [3]. The model requires six parameters and the value of each parameter used in this paper is given in Table 1. For clarity, the following section briefly describes the physical meanings of each parameter.

Table 1: Sand production model parameters used in this study

Parameter	Value
Stress reduction due to grain detachment ω_1	1.0
Rate of detachment ω_2	0.1 hour^{-1}
Critical gradient increase with hydrate ω_3	3.0
Shearing to potential conversion ω_4	1.0
Migrating solids settling/lifting ω_5	0
Critical gradient $i^{crit0}{}_w = i^{crit0}{}_g$	5.0

The model treats sand production roughly in three stages: detachment, migration and flowing into a well. First, solid grains are detached from soil skeletal continuum due to high hydraulic gradient exceeding its critical value. Secondly, the detached solids travel with fluid (water and/or gas) at the same superficial velocities, constituting solid-fluid mixtures. Thirdly, the migrating solids may settle or settled solids may be lifted and only the solids flowing into a well are considered as sand production. In the first stage, when a solid grain is detached, it is assumed to be from a part of soil skeletal continuum and thus it may temporarily cause the effective stress reduction (soon to be fully or partially recovered by mechanical deformation). The extent of reduction in the effective stresses is assumed to depend on the amount of detached solids and also the effective stresses carried by the soil skeleton. This mechanical-solid detachment coupling is governed by a parameter ω_1 as:

$$\frac{\partial \boldsymbol{\sigma}'}{\partial V_{ssi}} dV_{ssi} = \omega_1 \boldsymbol{\sigma}' \frac{dV_{ssi}}{V_{ssi}} \tag{1}$$

where $\boldsymbol{\sigma}$' is the effective stress vector and V_{ssi} is the volume of intact solids forming skeletal continuum and dV_{ssi} is the volume of detached solids (negative denotes detachment). The actual detachment occurs when the hydraulic gradient of water and/or gas exceeds its critical value. The detached volume is controlled by the amount of intact solids and detachability potential M^{dtc} (discussed later in Eq. (4)) such that:

$$dV_{ssi} = -V_{ssi}\omega_2 M^{dtc}\left[\frac{S_w}{S_w+S_g} H\left(\frac{i_w}{i_w^{crit}}-1\right)+\frac{S_g}{S_w+S_g} H\left(\frac{i_g}{i_g^{crit}}-1\right)\right]dt \tag{2}$$

where ω_2 is the parameter incorporating rate (time^{-1}), S is the saturation, $H(x)$ is the heaviside step function, i is the size of hydraulic gradient vector (i.e. $i = |\mathbf{i}|$), i^{crit} is the critical hydraulic gradient above which detachment of solid grain occurs, t is the time and the subscripts w and g represent water and gas, respectively. The relative pore occupancy in front of $H(x)$ for each medium facilitates the proportionality between water-driven and gas-driven detachment. The critical hydraulic gradient is assumed to increase with hydrate saturation as hydrates support neighboring grains and the suggested model utilizes the power function with a parameter ω_3:

$$i^{crit} = i^{crit0}(1-S_h)^{-\omega_3} \tag{3}$$

where i^{crit0} is the critical hydraulic gradient for grain detachment under single-phase (no hydrate) condition and ω_3 is the increasing factor with hydrate saturation S_h. The detachability potential introduced in Eq. (2) incorporates the effect of shearing deformation and a parameter ω_4 convers strain value to the detachability potential by:

$$M^{dtc} = \omega_4 \varepsilon_d + \ln\left(\frac{V_{ssi}}{V_{s0}}\right) \tag{4}$$

where ε_d is the deviatoric strain and V_{s0} is the initial intact solid volume (= V_{ssi0}). This model implies that grain detachment only occurs when there has been shearing deformation and the detachment ceases when the potential becomes zero even if the hydraulic gradient is above its critical value. At this point the volume of detached solids can be given by:

$$\Delta V_{ssi}^* = V_{ssi}^* - V_{s0} = V_{s0}\left[\exp\left(-\omega_4 \varepsilon_d\right)-1\right] \tag{5}$$

and the superscript * is added to represent "conditional", implying that this is the maximum detachable solid volume with the current value of ε_d and the magnitude of actual ΔV_{ssi} (= $V_{ssi} - V_{s0}$) is likely to be smaller as the potential may be greater than zero (i.e. $M^{dtc} > 0$) based on the fact that detachment may be currently ongoing due to low rate ω_2 or hydraulic gradient may be smaller than its critical value. The detached solids transport with the medium (water and/or gas) forming solid-fluid mixtures and their behavior is governed by Darcy's law. This is the second stage of the model, describing solid migration. In the third stage, the flowing solids may settle when the hydraulic gradient becomes lower than $\omega_5 i^{crit}$ ($0 \le \omega_5 \le 1$) or settled solids may be lifted again when the hydraulic gradient becomes greater than $\omega_5 i^{crit}$. For simplicity, this study ignores this settling/lifting process, i.e. $\omega_5 = 0$, and thus with time all

the migrating solids eventually flow into a well. Further details of the model, coupling manner and solving steps can be found in [3].

Near-wellbore numerical model geometry and initial conditions

In order to better investigate the effect of interbedded sand/clay layers on sand production, this paper employs near-wellbore modeling approach. Based on the conditions of a reservoir-scale model provided in a companion paper by the authors [4], this paper focuses on a thin layer out of 24.1 m thick hydrate-bearing sediments (Unit 4). The focused layer is assumed to be located 2850 m from the sea level and 280 m from the seabed, leading to the initial pore pressure and effective vertical stress of P_{w0} = 28.5 MPa and σ'_{z0} = 2.8 MPa, respectively. Two model geometries are considered: Case I - homogeneous hydrate-bearing sand layer; and Case II - sand/clay interbedded layers as illustrated in Fig. 1. Both cases are modeled using axisymmetric condition. The top and bottom sides of boundary is roller supported (i.e. smooth in the radial direction), facilitating a periodic boundary condition to incorporate the existence of hydrate-bearing sediments above and below. This leads to representations of, for Case I, sufficiently thick homogeneous hydrate-bearing sediments and, for Case II, a series of alternating sand and clay layers, the former has 1 m thickness and the latter has 0.2 m. The large number of alternating sand/clay layers are typically found in the Nankai hydrate site [5] and also considered in the 24.1 m thick hydrate-bearing layer presented in [4]. The size of the wellbore is r_0 = 0.15 m and the far-field boundary is set at r_∞ = 50 m. The domain is discretized into 30 elements in the radial direction, spanning the radial size from approximately 0.1 to 10 m. The wellbore boundary is mechanically-fixed in both directions but open for gas, water and sand productions. The far-field boundaries (i.e. far right-hand side in Fig. 1) are total stress controlled, that is, both the pore pressure and effective radial stress remain constant, which are in this study P_{w0} = 28.5 MPa and σ'_{r0} = 1.4 MPa, respectively. The initial temperature is T_0 = 19.4°C and the well is assumed to be insulated. Since the top and bottom boundaries are periodic, convection and conduction are only from the far-field boundary where the pore pressure and temperature remain constant.

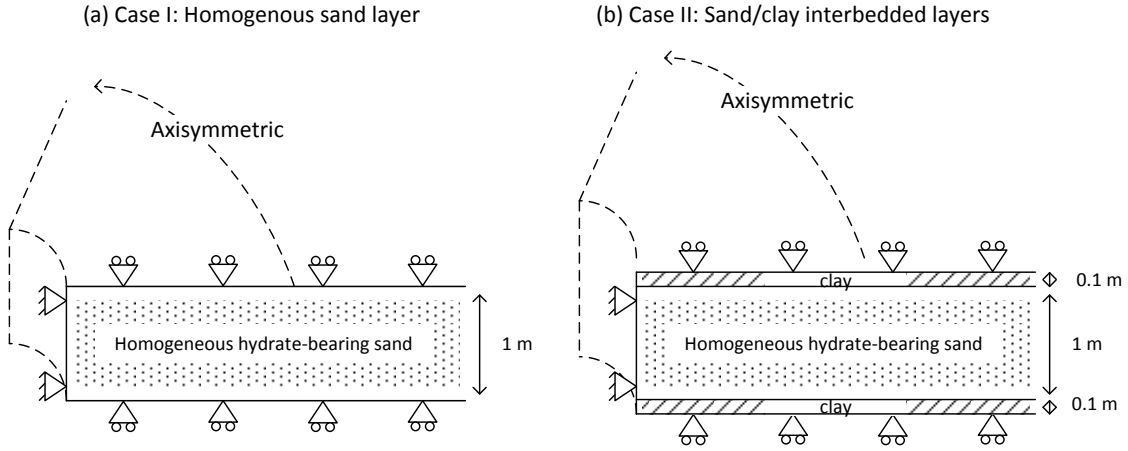

Figure 1: Model geometry representing a part of 24.1 m thick hydrate-bearing sediments (Unit 4)

Hydrates are assumed to exist only in the sand layer, forming homogeneous hydrate-bearing sand, and the initial hydrate saturation is S_{h0} = 80 %. The well pressure decreases to 8.5 MPa (i.e. 20 MPa pressure drawdown) by two days. Under the initial conditions the hydrate phase equilibrium pressure is 20.8 MPa. This means that the hydrates start to dissociate after 0.77 days into well depressurization.

Soil properties and other physical properties

For modeling of mechanical behavior of hydrate-bearing sand, this study utilizes the methane hydrate critical state constitutive model [6]. The model captures both shear yielding and volumetric yielding, the latter is particularly important under depressurization scheme. The clay layer is also modelled by the same model (with different parameters). For sand, the model is calibrated against the drained triaxial test data of synthetic hydrate-bearing sands recovered from the Nankai hydrate site by [7] and, for clay, the undrained triaxial test data on clays recovered from the Nankai hydrate site by [8]. For better representation, both shearing and volumetric behaviors are matched and the results are shown in Fig. 2. The calibrated soil properties/parameters are summarized in Table 2.

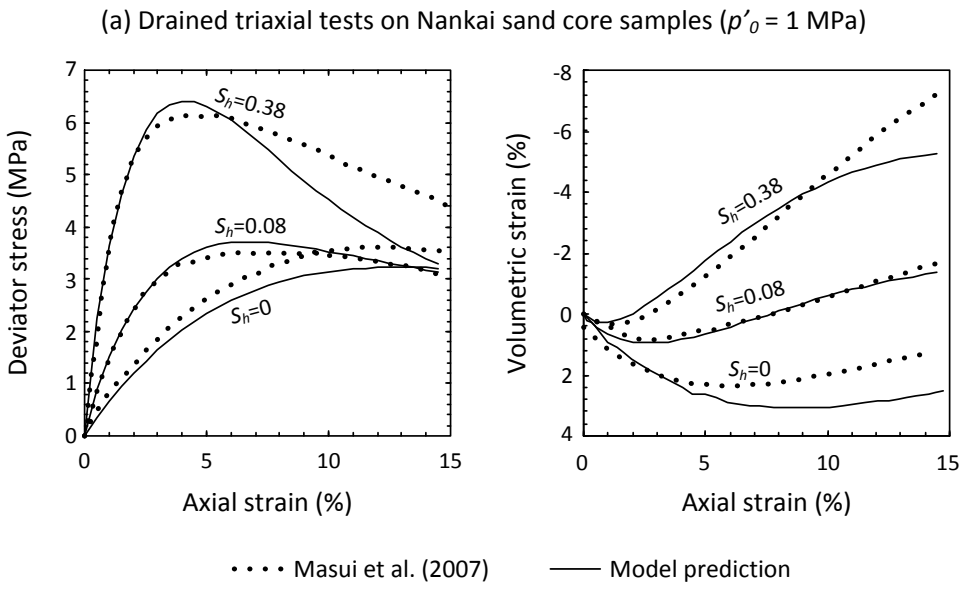

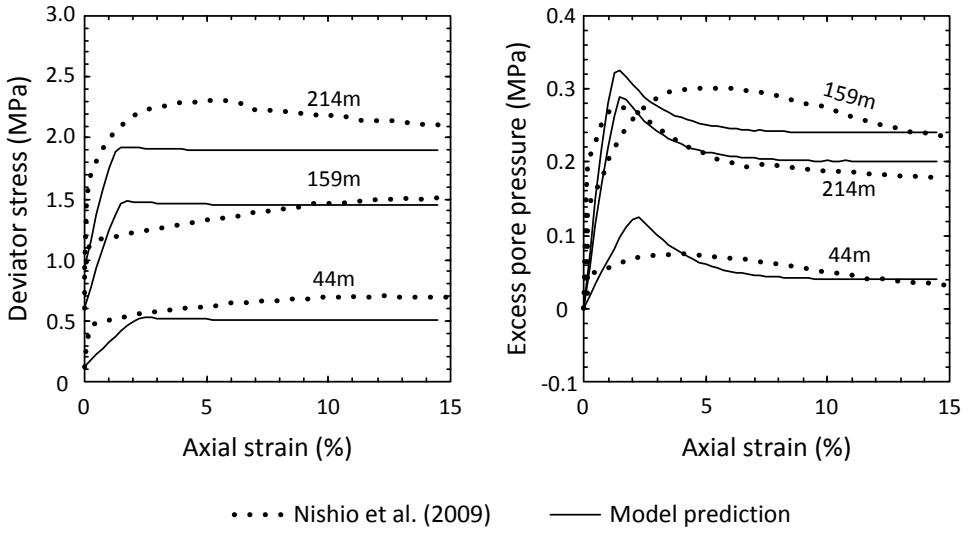

Fig. 2: Soil model calibration against existing laboratory test data

Table 2: Soil properties/parameters used in this study

Parameter	Hydrate-bearing sand	Clay
Initial void ratio e_0	0.54	0.54
Stress ratio at critical state M	1.40	1.32
Compression line λ	0.16	0.20
Swelling line κ	0.025	0.050
Poisson's ratio ν	0.28	0.23
Preconsolidation stress p'_{cs}	5.0 MPa	3.9 MPa
Subloading factor u	2.30	6.87
Hydrate dependent strength p'_{cd}	$45(S_h^{mec})^{0.8}$ MPa	-
Hydrate dependent modulus E_{h0}	320 MPa	-
Mechanical hydrate degradation m	15	-

The initial intrinsic permeability for sand is $||\mathbf{K}_0|| = 10^{-12}$ m^2 (1000 mD) and 5×10^{-19} m^2 (5×10^{-4} mD) for clay. These values increase/decrease with increase/decrease in the void volume based on the incremental form of Kozeny-Carman equation presented in [3]. The void volume changes can be caused by solid migration and volumetric deformation. For hydrate-bearing sand, the effective permeability is modeled by using a power law:

$$\mathbf{K}_h = \mathbf{K}(1 - S_h)^N \tag{6}$$

and in this study $N = 4.2$ is used, leading to the initial effective permeability of $||\mathbf{K}_{h0}|| \approx 10^{-15}$ m^2 (1mD) for the hydrate-bearing sand layer. This value increases with hydrate dissociation but the overall permeability is controlled by the combination of solid migration, volumetric deformation and hydrate dissociation. The other physical properties such as relative permeability relations [9] and the thermal conductivity are presented in [3].

Results and discussions

Thermo-hydro-mechanical responses

Fig. 3 shows the thermo-hydro-mechanical responses of the Case I sediments in near wellbore (consisting of 20 elements in the radial direction from r = 0.15 to 4.5 m) at t = 5, 10 and 30 days. As expected, depressurization induces hydrate dissociation, dropping the temperature and causing sediment deformation. The volumetric deformation is caused by the increase in the effective stresses due to pore pressure reduction. The deviatoric strain develops as the sediment deforms towards the well, causing shear stressing (i.e. reducing the effective radial stress σ'_r and increasing the effective circumferential stress σ'_θ). In addition, sediment deformation further develops due to reduction in soil strength and stiffness caused by hydrate dissociation. This can be seen by the development of strains from t = 10 to 30 days during which the hydrate saturation reduces while the pore pressure remains almost unchanged. Comparing the magnitudes of volumetric and deviatoric strains, it can be said that the sediments deform in more volumetric manner, highlighting the importance of incorporation of volumetric yielding.

Fig. 4 presents the thermo-hydro-mechanical responses of the Case II sediments. Compared with the homogenous case (Fig. 3), the presence of a thin clay layer tends to significantly affect the responses of the sediments. Most notably, hydrate dissociation preferentially occurs along the clay layer. This is because the clay layer constitutes heat source to drive hydrate dissociation as it remains relatively hotter than the sand layer. As a result, a larger volumetric strain develops along the sand/clay layer interface. This causes the sediments to deform towards the well as continuum and thus the sand layer away from the clay layer also deforms in a volumetric manner, effectively increasing the hydrate saturation (by reducing void ratio). This, in return, reduces the permeability in the sand layer as well as heat source via convection from far field and slows the process of hydrate dissociation away from the clay layer. This cycle amplifies the preferential hydrate dissociation pattern. These are evident from Figs. 4a-4d.

As mentioned previously, hydrate dissociation contributes to sediment deformation. When hydrate dissociates unevenly at a given radius, another important aspect of mechanical characteristic in hydrate-bearing sediments becomes relevant, that is, hydrate dissociation-induced stress relaxation. Since hydrates in pores carry the effective stresses, they temporarily release the effective stresses upon dissociation. The released effective stresses are soon recovered to reach a new stress equilibrium state by deformation, accompanying effective stress development in the neighboring sediments. In other words, sediments with dissociating hydrate pass the effective stresses onto sediments with higher hydrate saturation, causing additional deformation in the sediment with higher hydrate saturation. This unique feature can be found by comparing Fig. 3e and Fig. 4e. Near wellbore, for example, the interbedded sediment shows a greater deviatoric strain by 4 % compared to the homogenous sediment after it completely loses hydrate (i.e. S_h = 0). The difference comes from the fact that the interbedded sediment has carried more effective stresses than the homogenous sediment and the additional stresses have been transferred from the hydrates in the neighboring sediments. This difference highlights the importance of rigorous modeling of interbedded sediments to capture heterogeneous nature of hydrate dissociation pattern.

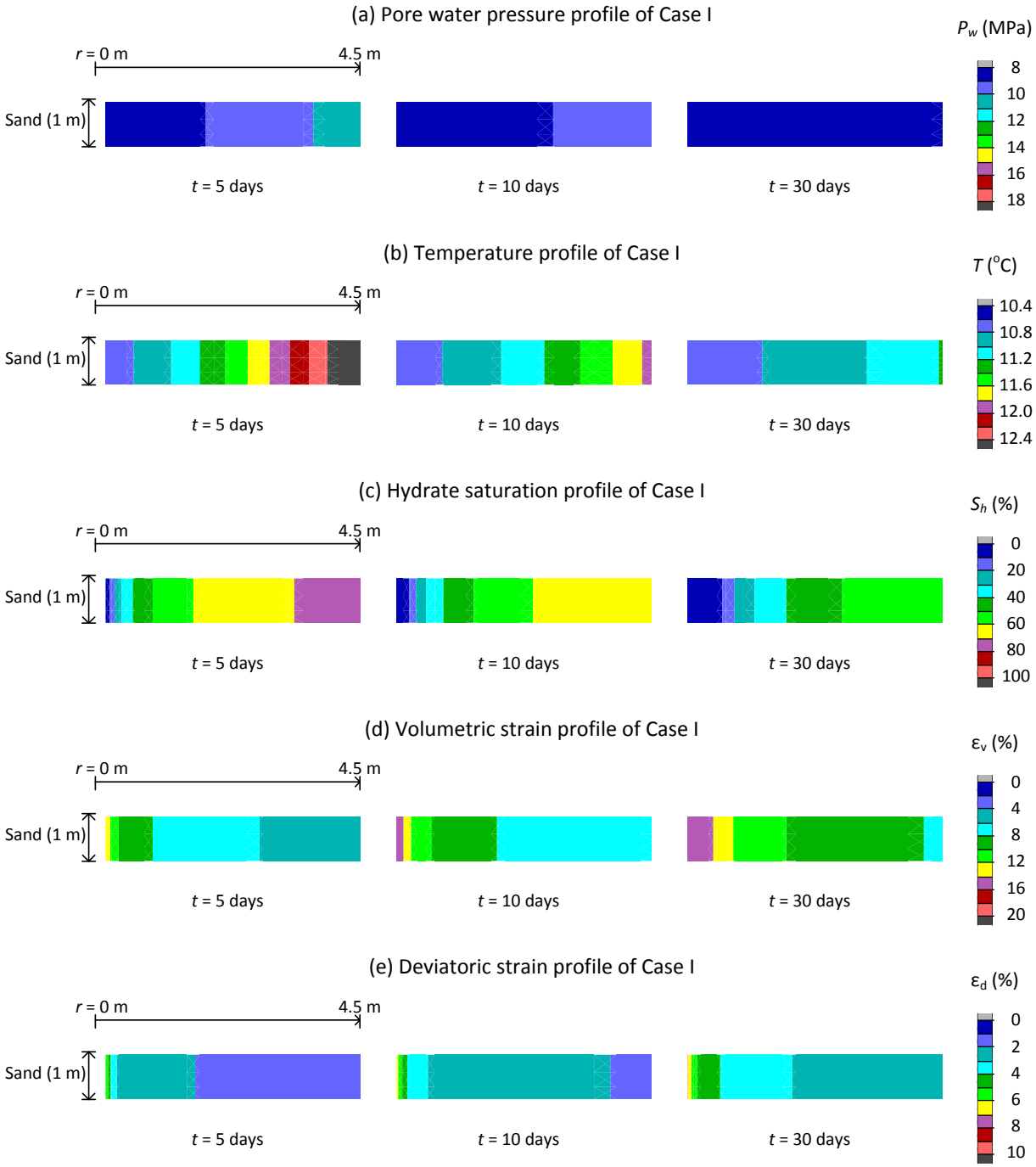

Figure 3: Thermo-hydro-mechanical responses of the Case I sediments near wellbore

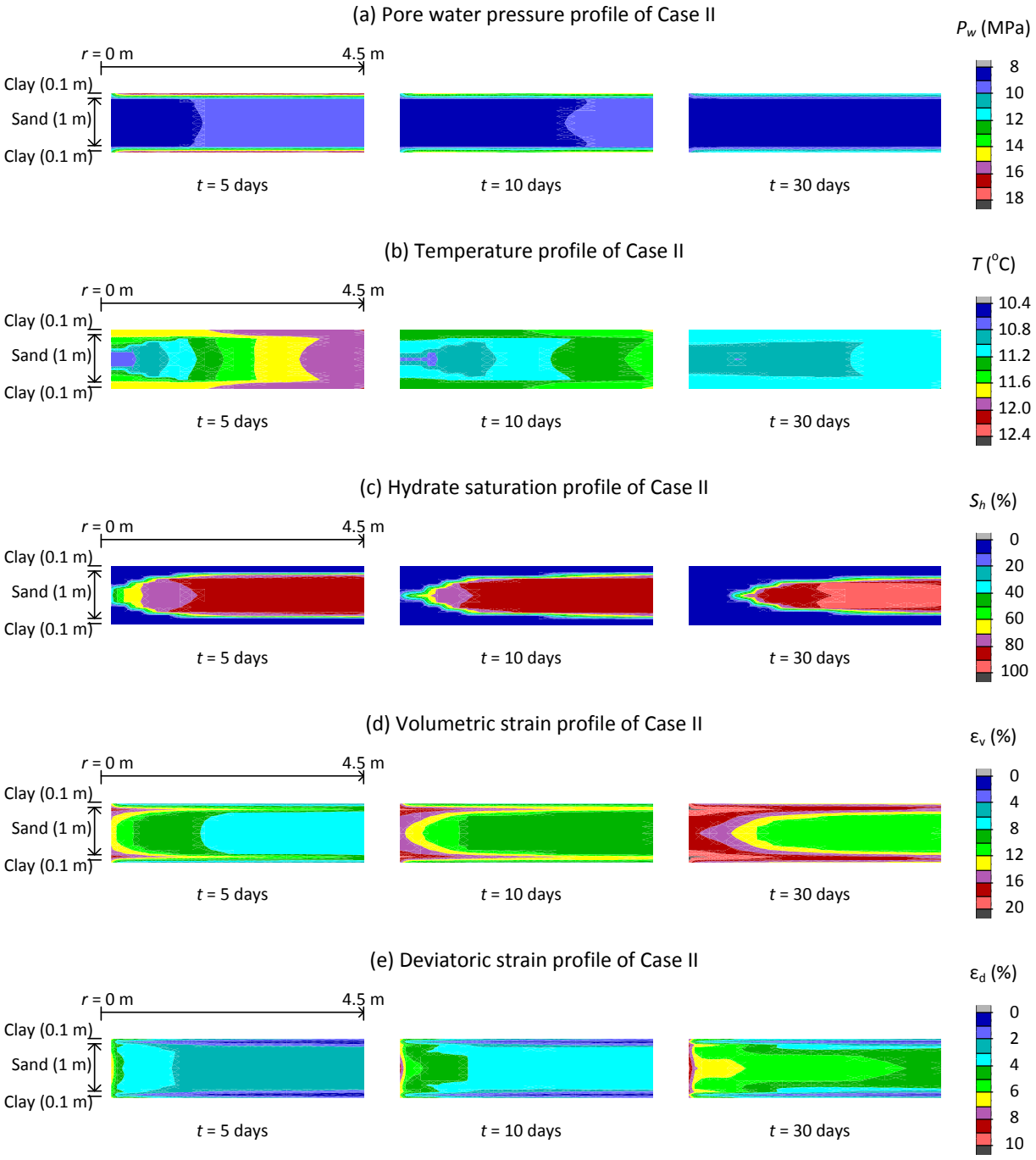

Figure 4: Thermo-hydro-mechanical responses of the Case II sediments near wellbore

Sand production studies

Fig. 5 shows (a) the ratio of hydraulic gradient of water to its critical gradient in logarithmic scale, $\ln(i_w/i^{crit}_w)$; and (b) the volume of detached solids from $t = 0$ to the specified time normalized by the initial solid volume, $\Delta V_{ssi}/V_{s0}$. The positive values in Fig. 4a indicate the areas where detachment can occur and these areas appear to reduce from $r \approx 4.5$ m at $t = 5$ days to $r \approx 2.7$ m at $t = 30$ days. Following two mechanisms contribute to this reduction: - one is that the hydraulic gradient is greater in the early stage of depressurization and the other is that hydrate dissociation increases the permeability and in return decreases the hydraulic gradient at a given pressure gradient. Since the hydraulic gradient is always greater than the critical value near the wellbore ($r < 2.0$ m), the volume of detached

solids increases with time as shown in Fig. 5b. This is because the shearing deformation keeps developing as hydrate dissociates (as shown in Fig. 3e), increasing the detachability potential as described in Eq. (4). In the middle region (2.0 m < r < 3.6 m) the detached solid volume does not significantly increase because of little development in deviatoric strain. In the areas away from the wellbore (3.6 m < r), the detached solid volume remains the same from t = 5 days onwards. This is because hydraulic gradient is lower than its critical value. Detailed studies show the flowing solids present at those selected times are negligibly small ($V_{fs}/V_{s0} \approx 10^{-5}$-$10^{-4}$), implying the detached solids migrate and flow into a well in a relatively short time.

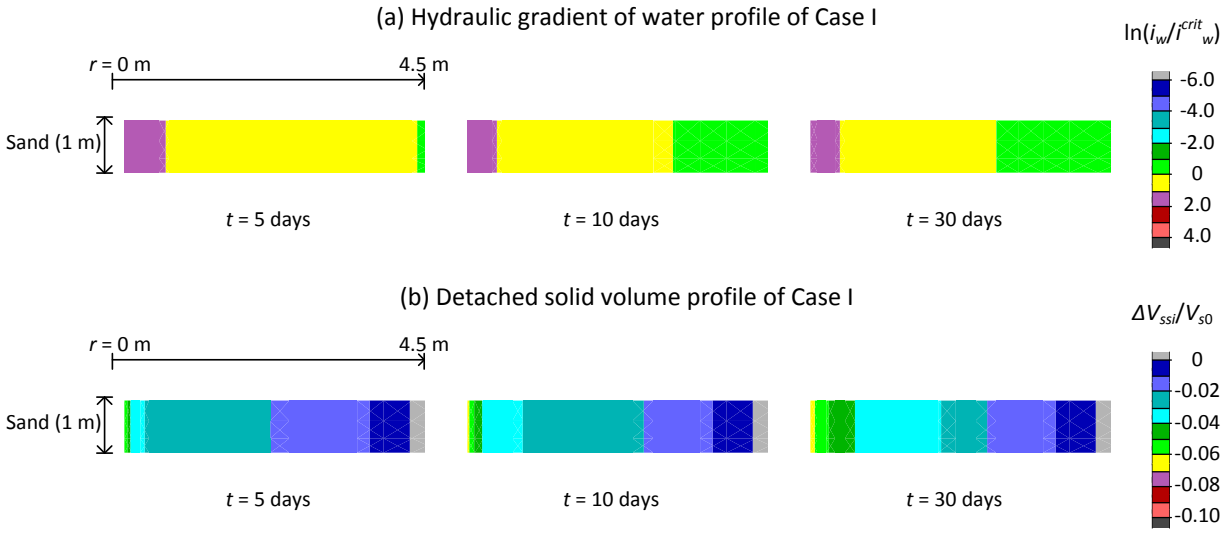

Figure 5: Sand production related properties in Case I

Fig. 6 shows the sand production related properties in Case II. Since hydrate dissociation occurs more locally near the sand/clay layers, more detached solids are evident along the sand/clay layers. Grain detachment is not modeled in the clay layer and thus the detached solids are entirely from the sand layer. The magnitude of detached volume itself is greater compared to the homogeneous case and this is attributed to the greater shearing deformation (Fig. 4e). Grain detachment does not occur where the hydrates remain in a relatively high amount even though there is detachability potential. This is because hydraulic gradient remains lower than the critical value. However, as the trend suggests, these areas would eventually induce grain detachment, starting from the perimeter of the remaining hydrates. Ongoing deviatoric deformation together with increase in the hydraulic gradient ratio i_w/i^{crit}_w, it is likely that detachment of solids continues and expands the areas to those away from the wellbore.

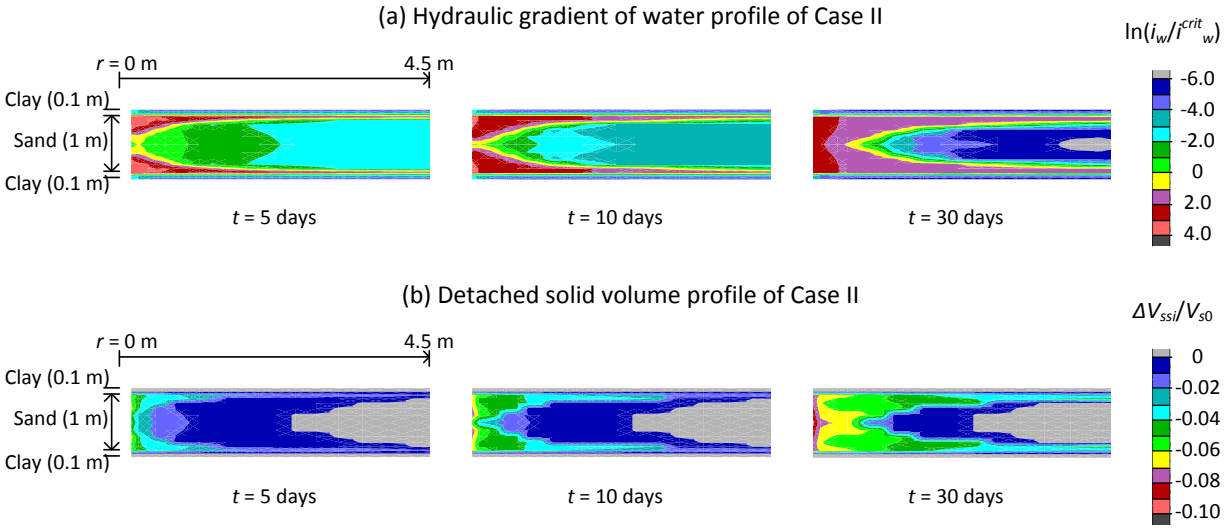

Figure 6: Sand production related properties in Case II

Fig. 7 presents the production of gas, water and sand from a unit height of the well for both Case I and Case II scenarios. The presence of a thin clay layer appears to contribute to all productions. It is interesting to state that by converting the produced volumes in a unit height for Case II (from 1.2 m to 1 m), it effectively reduces the amount of the hydrate in the considered domain but the produced gas volume is greater in Case II (Fig. 7a). This shows how beneficial the presence of a thin clay layer is for gas production. In terms of sand production, however, the presence of the clay layer intensifies sand production. While in Case I sand production appears to stabilize in the very early stage (around 4 days), in Case II sand production appears to continue even after 30 days as shown in Fig. 7c. The step-wise increase in the produced sand volume is likely to be numerical domain discretization artefact but the rate of sand production over a period of 30 days, that is, approximately 0.05 m^3/m per day, is found to be almost independent of finer/coarser discretization. Although the actual amount of sand production may vary with selected values of the parameter, this results show the adverse effect of a thin clay layer on sand production.

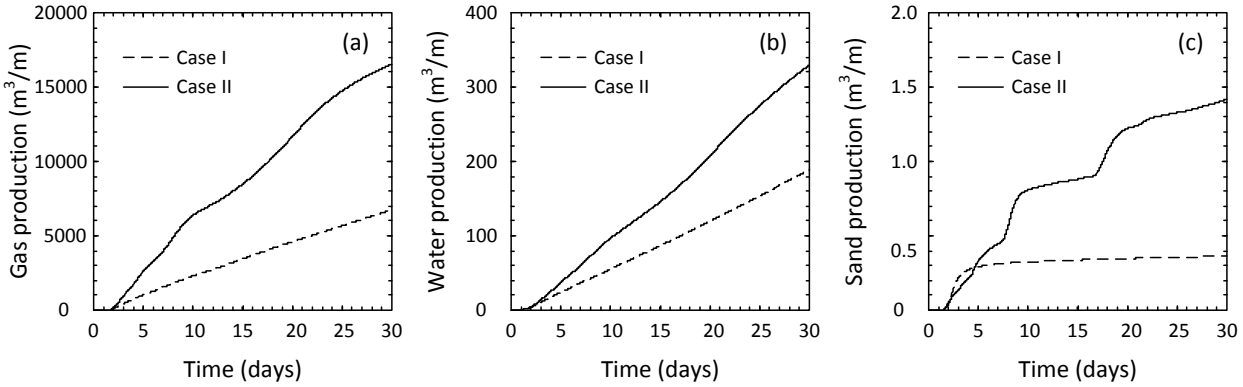

Figure 7: Production of (a) gas; (b) water; and (c) sand from Case I and Case II

Concluding remarks

This paper presented near-wellbore numerical analyses of homogenous hydrate-bearing sand and sand/clay interbedded hydrate-bearing sediments subjected to depressurization. The numerical analyses focused on the cause and effect of sand production using a coupled thermo-hydro-mechanical sand production model in hydrate-bearing sediments. It was found that greater sand production occurred when the interbedded sand/clay layers were present because of greater shearing deformation and locally high ratios of the hydraulic gradient to the critical gradient for grain detachment along the sand/clay interface. Both mechanisms were attributed to hydrate dissociation and thus it is important to accurately capture the heterogeneous nature of hydrate dissociation pattern. Although the amount of produced sand may vary with selected values of sand production related parameters, this finding implies that there would be a higher risk of excessive sand production if the production zone consists of a large number of sand/clay interbedded layers.

Acknowledgment

This technical effort was performed in support of the National Energy Technology Laboratory's ongoing research under the RES contract DE-FE0004000.

Disclaimer

This project was funded by the Department of Energy, National Energy Technology Laboratory, an agency of the United States Government, through a support contract with AECOM. Neither the United States Government nor any agency thereof, nor any of their employees, nor AECOM, nor any of their employees, makes any warranty, expressed or implied, or assumes any legal liability or responsibility for the accuracy, completeness, or usefulness of any information, apparatus, product, or process disclosed, or represents that its use would not infringe privately owned rights. Reference herein to any specific commercial product, process, or service by trade name, trademark, manufacturer, or otherwise, does not necessarily constitute or imply its endorsement, recommendation, or favoring

by the United States Government or any agency thereof. The views and opinions of authors expressed herein do not necessarily state or reflect those of the United States Government or any agency thereof.

References

[1] S.R. Dallimore, J. F. Wright, K. Yamamoto, G. Bellefleur, "Proof of concept for gas hydrate production using the depressurization technique, as established by the JOGMEC/NRCan/Aurora Mallik 2007-2008 Gas Hydrate Production Research Well Program", *Bulletin of the Geological Survey of Canada* 601: 1-15, 2012

[2] K. Yamamoto, Y. Terao, T. Fujii, I. Terumichi, M. Seki, M. Matsuzawa, T. Kanno, "Operational overview of the first offshore production test of methane hydrates in the Eastern Nankai Trough", *Offshore Technology Conference*: 25243MS, 2014

[3] S. Uchida, A. Klar, K. Yamamoto, "Sand production model in gas hydrate-bearing sediments", *International Journal of Rock Mechanics and Mining Sciences* 86: 303-316, 2016

[4] E. Myshakin, J.-S. Lin, S. Uchida, Y. Seol, T. Collett, R. Boswell, "Numerical studies of depressurization-induced gas production from an interbedded marine turbidite gas hydrate reservoir model", *ICGH9*, 2017

[5] K. Yamamoto, "Overview and introduction: Pressure core-sampling and analyses in the 2012–2013 MH21 offshore test of gas production from methane hydrates in the eastern Nankai Trough", *Marine and Petroleum Geology* 66(2): 296–309, 2015

[6] S. Uchida, X.-G. Xie, Y.F. Leung, "Role of critical state framework in understanding geomechanical behavior of methane hydrate-bearing sediments", *Journal of Geophysical Research* 121(8): 5580-5595, 2016.

[7] A. Masui, H. Haneda, Y. Ogata, K. Aoki, "Mechanical properties of sandy sediment containing marine gas hydrates in Deep Sea Offshore Japan Survey drilling in Nankai Trough", *Seventh ISOPE Ocean Mining Symposium*: 55-56, 2007

[8] S. Nishio, E. Ogisako, A. Denda, "Geotechnical properties of core samples recovered from seabed ground in East Nankai Trough", *Journal of Geography* 118(5): 955-968, 2009 [in Japanese]

[9] M. van Genuchten, "A closed form equation for predicting the hydraulic conductivity of unsaturated soils", *Soil and Science Society of America Journal* 44: 892-898, 1980